Journal of Physiology and Biochemistry (2023) 79:731–743
https://doi.org/10.1007/s13105-023-00970-4

ORIGINAL ARTICLE

Hepatocellular carcinoma induced by hepatocyte Pten deletion reduces BAT UCP-1 and thermogenic capacity in mice, despite increasing serum FGF-21 and iWAT browning

Álbert S. Peixoto[1] · Mayara F. Moreno[1] · Érique Castro[1] · Luiz A. Perandini[1] · Thiago Belchior[1] · Tiago E. Oliveira[1] · Thayna S. Vieira[1] · Gustavo R. Gilio[1] · Caroline A. Tomazelli[1] · Bianca F. Leonardi[1] · Milene Ortiz-Silva[1] · Luciano P. Silva Junior[1] · Eduardo H. Moretti[2] · Alexandre A. Steiner[2] · William T. Festuccia[1]

Received: 10 December 2022 / Accepted: 23 June 2023 / Published online: 5 July 2023

Abstract

Hepatocellular carcinoma (HCC) markedly enhances liver secretion of fibroblast growth factor 21 (FGF-21), a hepatokine that increases brown and subcutaneous inguinal white adipose tissues (BAT and iWAT, respectively) uncoupling protein 1 (UCP-1) content, thermogenesis and energy expenditure. Herein, we tested the hypothesis that an enhanced BAT and iWAT UCP-1-mediated thermogenesis induced by high levels of FGF-21 is involved in HCC-associated catabolic state and fat mass reduction. For this, we evaluated body weight and composition, liver mass and morphology, serum and tissue levels of FGF-21, BAT and iWAT UCP-1 content, and thermogenic capacity in mice with Pten deletion in hepatocytes that display a well-defined progression from steatosis to steatohepatitis (NASH) and HCC upon aging. Hepatocyte Pten deficiency promoted a progressive increase in liver lipid deposition, mass, and inflammation, culminating with NASH at 24 weeks and hepatomegaly and HCC at 48 weeks of age. NASH and HCC were associated with elevated liver and serum FGF-21 content and iWAT UCP-1 expression (browning), but reduced serum insulin, leptin, and adiponectin levels and BAT UCP-1 content and expression of sympathetically regulated gene glycerol kinase (GyK), lipoprotein lipase (LPL), and fatty acid transporter protein 1 (FATP-1), which altogether resulted in an impaired whole-body thermogenic capacity in response to CL-316,243. In conclusion, FGF-21 pro-thermogenic actions in BAT are context-dependent, not occurring in NASH and HCC, and UCP-1-mediated thermogenesis is not a major energy-expending process involved in the catabolic state associated with HCC induced by Pten deletion in hepatocytes.

Keywords Nonalcoholic fatty liver disease · Energy expenditure · UCP-1 · Thermogenic capacity · Brown adipose tissue · White adipose tissue browning

Key points
- Hepatocellular carcinoma reduces BAT UCP-1 content and thermogenic capacity
- Thermogenic capacity was reduced despite increased serum FGF-21 and iWAT browning
- Pro-thermogenic actions of FGF-21 are context-dependent
- iWAT browning does not compensate for reduced BAT thermogenic capacity

✉ William T. Festuccia
william.festuccia@usp.br; william.festuccia@gmail.com

[1] Department of Physiology and Biophysics, Institute of Biomedical Sciences, University of Sao Paulo, Av. Prof Lineu Prestes, 1524, 05508000 Sao Paulo, Brazil

[2] Department of Immunology, Institute of Biomedical Sciences, University of Sao Paulo, Sao Paulo, Brazil

Introduction

Liver steatosis, defined as lipid deposition in hepatocytes exceeding 5 to 10% of the liver mass, is a common phenotype found in a group of liver complications collectively known as nonalcoholic fatty liver disease (NAFLD) [44]. NAFLD comprises simple steatosis (NAFL) to the more severe diseases steatohepatitis (NASH), cirrhosis, and hepatocellular carcinoma (HCC) [44]. NAFLD affects between 25 and 45% of people worldwide, and its incidence and prevalence are globally rising owing to the increasing rates of obesity and type 2 diabetes [44]. Noteworthy, NAFLD can be also found in lean patients with a body mass index

lower than 25 due to enhanced visceral fat accumulation or lipodystrophy, among other reasons [1].

Lipid accumulation in hepatocytes, the primary triggering event in NAFLD, occurs when rates of fatty acid uptake and de novo synthesis exceed rates of fatty acid oxidation and export as very low-density lipoprotein (VLDL)-triacylglycerol [46]. Generally, liver lipid accumulation occurs as the result of impaired adipose tissue lipid storage and/or excessive lipolysis and, therefore, enhanced lipid flux to the liver, as well as enhanced hepatic de novo fatty acid synthesis (lipogenesis) and insulin resistance [46].

Along with lipid metabolism, NAFLD also impacts liver endocrine function and secretion of hepatokines, hormones that communicate liver metabolic status to the central nervous system and peripheral organs [25]. Tsukushi (TSK), for instance, a hepatokine that is highly secreted in patients with steatosis and acetaminophen-injured liver was shown to regulate cholesterol homeostasis and conversion to bile acids [38]. Whether TSK also regulates glucose homeostasis, brown fat thermogenesis, and energy expenditure is still a matter of debate [37, 55]. Furthermore, liver production and secretion of fibroblast growth factor 21 (FGF-21), a member of the FGF-19 subfamily, are increased in several mouse models of NASH and HCC induced either chemically (diethylnitrosamine) or genetically (hepatocyte deletions of Pten, LKB1, p53, etc.) [57], as well as in patients with either NAFL or NASH [14], reflecting liver steatosis score and strongly predicting hepatic steatosis stage [58]. The mechanisms driving liver FGF-21 secretion upon NAFLD were not completely defined yet, but they may involve activation of the transcription factors p53, signal transducer and activator of transcription 3 (STAT3), carbohydrate-responsive element-binding protein (ChREBP), and peroxisome proliferator-activated receptor α (PPARα) in response to stress, cytokines, sucrose, and lipids [17, 2, 57], among other factors. FGF-21 has important actions on energy balance and thermoregulation, reducing body weight and NAFLD and increasing energy expenditure and body temperature, such effects that are in part due to an upregulation of brown and white adipose tissue (BAT and WAT, respectively), uncoupling protein 1 (UCP-1) content and mediated thermogenesis [59, 56, 12]. Higher hepatic FGF-21 secretion upon NAFLD may be considered, therefore, a compensatory mechanism to counteract liver lipid deposition and steatosis.

Considering FGF-21 robust pro-thermogenic actions and enhanced secretion upon HCC, as well as the previous speculation that UCP-1-mediated thermogenesis may promote cancer-associated cachexia [50, 19, 29], we tested herein the hypothesis that an enhanced BAT and subcutaneous inguinal WAT (iWAT) UCP-1-mediated thermogenesis induced by high levels of FGF-21 are involved in the catabolic state and reduction in fat mass associated with HCC. To test this, we evaluated energy balance, serum and tissue FGF-21, BAT and iWAT UCP-1 content, and thermogenic capacity in mice with Pten deletion in hepatocytes, which develop independently of diet, chemical agents, and other external confounding factors that could independently affect BAT function, a well-defined temporal NAFL-NASH-HCC progression due to the constitutive activation of PI3K-mTORC2-Akt-mTORC1 signaling [21, 52]. Noteworthy, mutations or single nucleotide polymorphisms (SNPs) that inactivate Pten and, therefore, constitutively activate PI3K-mTORC2-Akt-mTORC1 signaling are closely associated with the development of steatosis and HCC in humans [3, 11], while whole-body Pten overexpression protects mice from NAFLD [42]. Furthermore, reduced liver Pten expression and protein content are common features found in rodent models of NAFLD (the Zucker diabetic fatty and high-fat-fed Wistar rats) and patients with steatosis [53], as well as human hepatocarcinoma cell lines and liver samples [23]. Finally, homozygous deletion of Pten is a recurrent genetic signature found in HCC [18, 47].

Materials and methods

Mice

Mice experimental procedures were conducted at the Laboratory of Molecular Physiology and Metabolism, Institute of Biomedical Sciences, University of Sao Paulo, after approval by the Animal Care Committee of the Institute of Biomedical Sciences, University of Sao Paulo (#115/2016 and 6160250820, CEUA). All mice used were on a C57BL/6J background. *Pten*$^{Lox/Lox}$ mice (B6.129S4-*Pten*^{tm1Hwu}/J, Jackson Laboratories) were crossed to albumin-cre mice (B6.Cg-*Speer6-ps1*$^{Tg(Alb-cre)21Mgn}$/J, Jackson Laboratories) to obtain heterozygous *Pten*$^{Lox/WT}$; albumin-cre$^{+/-}$ offspring (where WT refers to wild type) in the F1 generation. These heterozygous mice were crossed with *Pten*$^{Lox/Lox}$ mice to obtain mice with the genotype *Pten*$^{Lox/Lox}$; albumin cre$^{+/-}$ (referred henceforth as L-Pten KO mice) and their littermates *Pten*$^{Lox/Lox}$; albumin cre$^{-/-}$ (referred henceforth as L-Pten WT). Mice genotypes were determined by PCR analysis of tail genomic DNA. Mice were kept at 23 ± 1 °C on a 12:12 h light-dark cycle, fed a nonpurified chow diet (70% carbohydrate, 20% protein, 10% fat, in % kcal, NUVILAB CR-1®-Sogorb Inc., Paraná, Brazil) and killed at 8, 24, and 48 weeks of age after 10 h of food deprivation (from 10:00 pm to 08:00 am) by cervical dislocation for tissue and blood harvesting after anesthesia with isoflurane. Body weight and food intake were measured weekly. Subcutaneous inguinal white adipose tissue (iWAT) was evaluated herein because it shows the higher propensity and capacity for browning in mice [54, 13, 48]. BAT, herein, refers to the interscapular depot only.

Indirect calorimetry

Mice were adapted to the metabolic cages for 2 consecutive days and evaluated for oxygen consumption (VO2), carbon dioxide production (VCO2), spontaneous motor activity, and respiratory exchange ratio (RER, VCO2/VO2 ratio) during 24 h in a comprehensive laboratory monitoring system calorimeter (Columbus Instruments) as previously described [40]. The relationship between oxygen consumption and body mass in 8-, 24-, and 48-week-old mice was evaluated using ANCOVA essentially as described [26, 27].

Tissue oxygen consumption

Explants from the liver, iWAT, and BAT were incubated in DMEM containing 2% BSA (w/v) under continuous stirring at 37 °C and evaluated for oxygen consumption in an Oroboros Oxygraph-2 K as described [34].

Mice oxygen consumption and body temperature in response to CL-316,243 (thermogenic capacity)

Mice, 48 weeks old, were anesthetized with isoflurane and placed on a heat pad warmed at 37 °C for the insertion of a temperature transmitter (model TA-F10; Data Sciences International, MN) in the peritoneal cavity. The abdominal wall was sutured, and the skin was closed with surgical glue (Dermabond Topical Skin Adhesive; Johnson & Johnson, Sao Paulo, Brazil). After surgery, mice were treated with antibiotic (enrofloxacin 5 mg/kg sc) and analgesic (ketoprofen 5 mg/kg sc) and allowed to recover for 7 days. After this period, mice were transferred to metabolic cages at 30 °C at 09:00 h and food restricted. After 3 h (12:00 h), mice were intraperitoneally injected with the β-adrenergic agonist CL-316,243 (1 mg/kg in PBS) and evaluated for body temperature and oxygen consumption. Core body temperature was monitored and acquired in continuous mode by the Data Sciences telemetry system. Oxygen consumption was determined by open-flow respirometry as described elsewhere [51]. A similar procedure was used to evaluate oxygen consumption in response to CL-316,243 in 8 weeks old mice, but without the surgery and insertion of a temperature transmitter.

FGF-21, leptin, insulin, and adiponectin

Serum FGF-21, leptin, insulin, and adiponectin levels were measured with mouse ELISA kits (FGF-21 DuoSet ELISA, R&D, MN, USA; and mouse leptin, adiponectin and ultra-sensitive mouse insulin from Crystal Chem, IL, USA) following supplier recommendations. For the evaluation of tissue FGF-21 content, liver, BAT, and iWAT were homogenized in a buffer composed of 50 mM HEPES, 2 mM EDTA, 10 mM sodium pyrophosphate, 40 mM NaCl, 10 mM sodium glycerophosphate, 50 mM NaF, 2 mM sodium orthovanadate, 1% Triton-X 100, and EDTA-free protease inhibitors and centrifuged. Supernatant was used for FGF-21 content measurement by ELISA.

RNA extraction and qPCR

Total RNA was extracted from the liver (30 mg), iWAT (100 mg), and BAT (40 mg), reverse transcribed, and destined for quantitative PCR analysis as previously described [34]. Primer nucleotide sequences are depicted in Table 1. Analysis of real-time PCR data was performed using the $2^{-\Delta\Delta CT}$ method. Data are expressed as the ratio between the expression of the target gene and the housekeeping genes (36B4 and RPL3), the expression of which was not significantly affected by the mouse genotype.

Liver histology

Liver, BAT, and iWAT samples were fixed in 4% paraformaldehyde and embedded in paraffin. Sections 5.0 µm-thick were obtained and stained with hematoxylin and eosin (H/E) to assess general liver morphology. Liver histopathological analysis was carried out using a previously defined NAFLD scoring system for rodents [32].

Table 1 Primers used in qPCR

Gene	NM number	Forward (5′-3′)	Reverse (3′-5′)
ChREBPα	NM_021455.5	CGACACTCACCCACCTCTTC	TTGTTCAGCCGGATCTTGTC
ChREBPβ	NM_001359237.1	TCTGCAGATCGCGTGGAG	CTTGTCCCGGCATAGCAAC
FATP1	NM_011977.4	GGCCACCATTCCTACAGCAT	CGTGAGGATACGGCTGTTGA
GyK	NM_008194.3	ATCCGCTGGCTAAGAGACAACC	TGCACTGGGCTCCCAATAAGG
LPL	NM_008509.2	TCGCCTTTCTCCTGATGACG	CTGGTCCACGTCTCCGAGT
PPARα	NM_001113418.1	CAGCCTCAGCCAAGTTGAAG	CACAGAGCGCTAAGCTGTGA
TSK	NM_001168541	TGCAGGGCATCCTCCATCTA	GCCTGAAAACACCTCAGCTC
UCP-1	NM_009463.3	AGGCTTCCAGTACCATTAGGT	CTGAGTGAGGCAAAGCTGATTT

Western blot analysis

BAT (30 mg) and iWAT (50 mg) were homogenized in a buffer composed of 50 mM HEPES, 2 mM EDTA, 10 mM sodium pyrophosphate, 40 mM NaCl, 10 mM sodium glycerophosphate, 50 mM NaF, 2 mM sodium orthovanadate, 1% Triton-X 100, and EDTA-free protease inhibitors, centrifuged, and analyzed for protein content as previously described [9]. Primary antibody against UCP-1 (#14670) (Cell Signaling Technology, Beverly, MA, USA) was diluted at 1:1000 in TBS-T 5% milk. Membranes were incubated with peroxidase-conjugated secondary antibody (1:5000) and revealed with ECL-enhanced chemiluminescence substrate (GE Healthcare).

Statistical analysis

Data are expressed as mean ± SEM. Student's *t*-test was used to analyze the effects of hepatocyte Pten deletion (same age L-Pten WT vs L-Pten KO) using GraphPad Prism. The significance level was set at $p \leq 0.05$.

Results

As illustrated in Fig. 1, mice with Pten deletion exclusively in hepatocytes displayed a gradual and robust increase in liver mass, lipid accumulation, and steatosis upon aging, as evaluated by H/E staining, culminating at 24 weeks in NASH and 48 weeks in hepatomegaly and development of liver tumors (Fig. 1A, B). Indeed, all 48 weeks old L-Pten KO evaluated displayed several tumors homogenously distributed all over the liver (Fig. 1A). Histopathologic analysis of L-Pten KO mouse liver revealed a clear NAFL-NASH-HCC progression upon aging characterized by increased steatosis score (sum of micro and macrovesicular steatosis and hepatocyte hypertrophy) and fibrosis (Fig. 1A and Table 2). Of note, inflammatory foci were found exclusively in the NASH (24 weeks) and HCC (48 weeks), but not NAFL displayed by L-Pten KO mice (Table 2).

Despite the marked increase in L-Pten KO liver mass, there were no differences in mice's body weight between groups (Fig. 1C). Indeed, L-Pten KO displayed reduced masses of iWAT (Fig. 1D) at 24 and 48 weeks of age and of gastrocnemius skeletal muscle at 48 weeks of age only (Fig. 1E). In contrast to iWAT and gastrocnemius, BAT mass was significantly increased in 8, 24, and 48 weeks old L-Pten KO (Fig. 1F). There were no differences in food intake between groups (Fig. 1G). Altogether, these findings indicate that mice bearing HCC induced by hepatocyte Pten deletion show increased liver and BAT but reduced iWAT and skeletal muscle masses, ensuring no changes in body weight.

Next, we investigated the impact of NAFLD progression on serum and tissue FGF-21 content. As illustrated in Fig. 2A, serum FGF-21 concentration was significantly increased in L-Pten KO upon aging and progression of liver disease, attaining its highest levels in 48-week-old HCC-bearing mice. A similar pattern was seen in liver FGF-21 content, namely, an increase upon aging and progression of liver disease (Fig. 2B). In contrast, FGF-21 content was either not altered in BAT or increased in iWAT, but only in 48-week-old L-Pten KO (Fig. 2C, D, respectively). Serum insulin and leptin were significantly reduced in L-Pten KO in all ages investigated (Fig. 2E, F), while serum adiponectin was reduced in 24- and 48-week-old L-Pten KOs only (Fig. 2G). Liver mRNA content of Tsukushi, a hepatokine secreted upon liver disease, was significantly increased in 24- and 48-week-old L-Pten KOs (Fig. 2H), while mRNA content of the transcription factors and regulators of FGF-21 expression, namely, ChREBPβ (all ages) and PPARα (8 and 48 weeks old), but not ChREBPα, was significantly increased in L-Pten KO mice (Fig. 2I–K). These findings indicate that NAFLD progression induced by hepatocyte Pten deletion increases serum FGF-21 levels mainly by increasing liver production and secretion of this hepatokine through a mechanism that may involve activation of ChREBPβ and PPARα.

Our findings that BAT mass and serum FGF-21 are increased in L-Pten KO mice motivate us to investigate the impact of NAFLD progression on BAT and iWAT thermogenic function. As illustrated in Fig. 3, fatty liver disease was associated with major changes in BAT and iWAT gene expression profile, uncoupling protein 1 (UCP-1) content, and tissue morphology. Indeed, L-Pten KO displayed in BAT reduced mRNA content of UCP-1 (Fig. 3A), glycerol kinase (GyK) (Fig. 3B), lipoprotein lipase (LPL) (Fig. 3C), and fatty acid transporter protein 1 (FATP-1) (Fig. 3D) at 8, 24, and 48 weeks of age; reduced protein content of UCP-1 at 24 and 48 weeks of age (Fig. 3E); and increased lipid deposition and percentage of unilocular cells at 8, 24, and 48 weeks of age (Fig. 3F). In contrast, L-Pten KO displayed in iWAT increased UCP-1 (Fig. 3G) and GyK (Fig. 3H) mRNA content at 24 and 48 weeks of age, but no changes in LPL (Fig. 3I) and FATP-1 (Fig. 3J) mRNA. Consistently with UCP-1 and GyK mRNA, histological analysis of iWAT revealed the appearance of multilocular adipocytes mainly in 48-week-old L-Pten KO (Fig. 3K). Altogether, these findings suggest that liver cancer induced by Pten deletion in hepatocytes impacts BAT and iWAT differently, with the former showing clear signs of inactivation and the latter featuring thermogenic recruitment and browning.

In the face of the opposite response of both BAT and iWAT seen in 48-week-old L-Pten KO, we next compared total UCP-1 content in both tissues to evaluate their

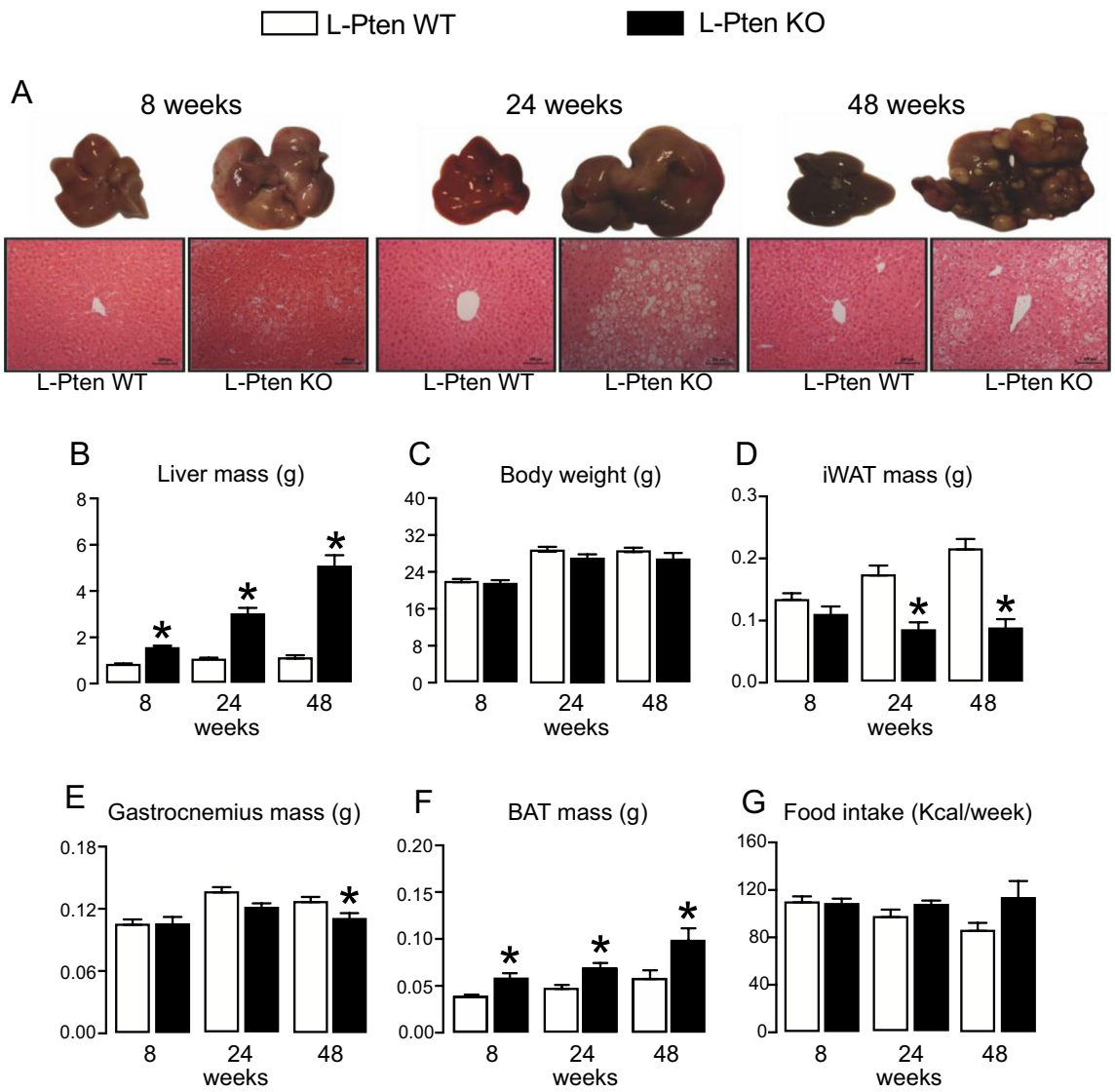

Fig. 1 Pten deletion in hepatocytes promotes liver cancer and reduces iWAT and gastrocnemius masses in 48-week-old mice. Liver mass (**A**) and microphotography and histology by H/E staining (**B**), body weight (**C**), inguinal white adipose tissue (iWAT) (**D**), gastrocnemius (**E**), and brown adipose tissue (BAT) (**F**) masses and food intake (**G**) in 8-, 24-, and 48-week-old Pten floxed (L-Pten WT) and Pten floxed albumin cre$^{+/-}$ (L-Pten KO) mice bearing Pten deletion in hepatocytes. Results are expressed as mean ± SEM. n = 6–16 mice per group. Student's t-test was used to analyze the effects of Pten deletion (same age L-Pten WT vs L-Pten KO). *$p \leq 0.05$

Table 2 Histopathological features of NAFLD in 8, 24, and 48 weeks-old mice with Pten deletion in hepatocytes (L-Pten KO) and littermate controls (L-Pten WT)

L-Pten	8 weeks		24 weeks		48 weeks	
	WT	KO	WT	KO	WT	KO
Macrovesicular steatosis	0	0	0	0.4	0	0.5
Microvesicular steatosis	0	1.5	0	2.4	0	2.2
Hepatocellular hypertrophy	0	1.2	0	2.2	0	0.7
Inflammation	0	0	0	1.3	0	2
Steatosis score	0	2.7	0	5.0	0	3.4

Macrovesicular and microvesicular steatosis and hepatocellular hypertrophy, defined as cellular enlargement >1.5 times the normal hepatocyte diameter, were scored based on the percentage of the total area affected: 0 (<5%), 1 (5–33%), 2 (34–66%), and 3 (>66%). Inflammation was evaluated by counting the number of inflammatory foci per field. Steatosis score is the sum of macrovesicular plus microvesicular steatosis plus hepatocellular hypertrophy

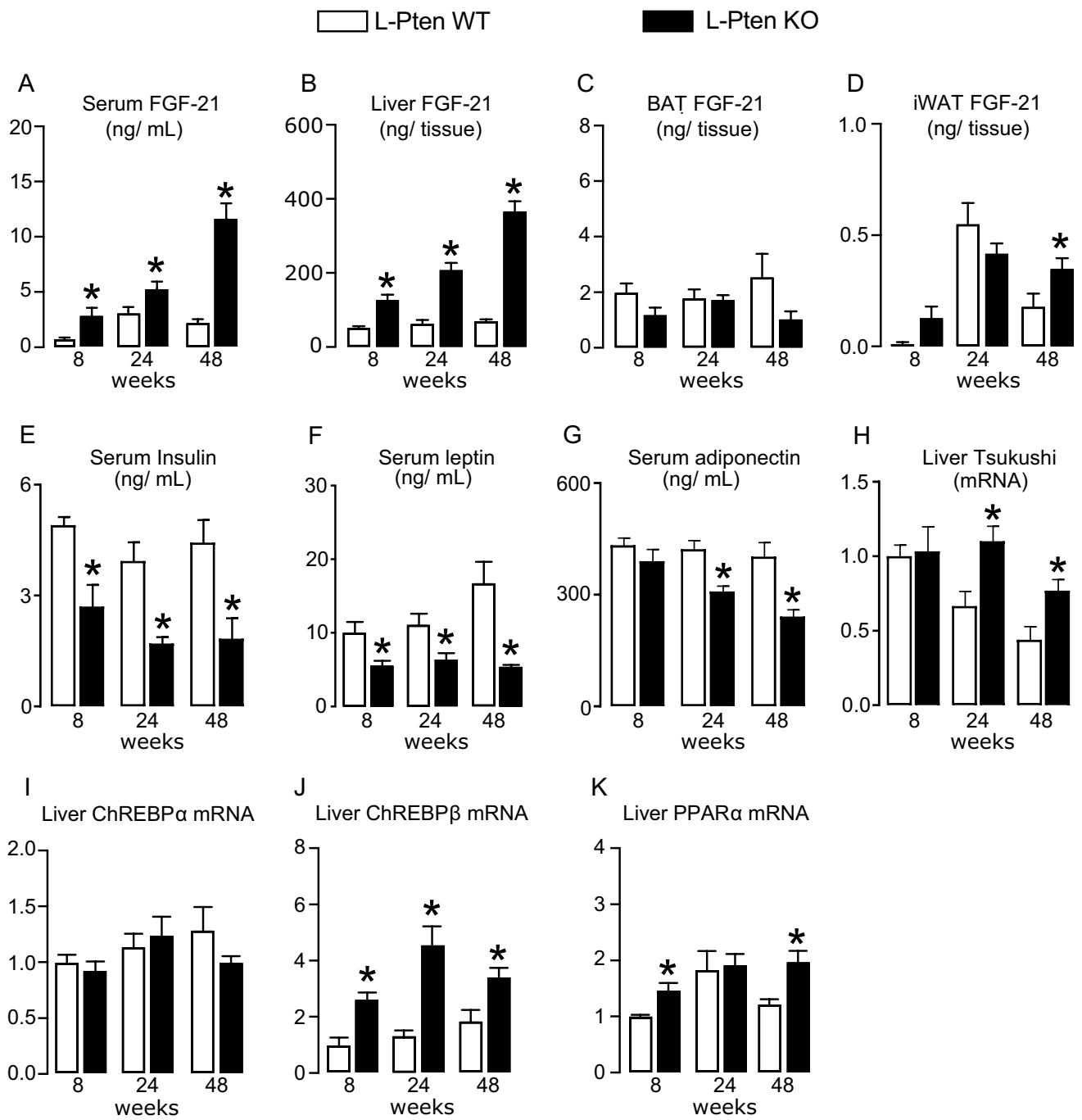

Fig. 2 NAFLD induced by Pten deletion in hepatocytes is associated with increased serum and liver FGF-21 content and Tsukushi, ChREBPβ, and PPARα mRNA but reduced serum insulin, leptin, and adiponectin levels. Serum (**A**), liver (**B**), brown adipose tissue (BAT) (**C**), and inguinal white adipose tissue (iWAT) (**D**) FGF-21 content, serum insulin (**E**), leptin (**F**), adiponectin (**G**) levels and liver Tsukushi (**H**), ChREBPα (**I**), ChREBPβ (**J**), and PPARα (**K**) mRNA content in 8-, 24-, and 48-week-old Pten floxed (L-Pten WT) and Pten floxed albumin cre$^{+/-}$ (L-Pten KO) mice bearing Pten deletion in hepatocytes. Results are expressed as mean ± SEM. n = 5-8 mice per group. Student's t-test was used to analyze the effects of Pten deletion (same age L-Pten WT vs L-Pten KO). *$p \leq 0.05$

individual impact on whole-body energy expenditure. As illustrated in Fig. 4A, applying the same amount of protein, we did not detect UCP-1 in iWAT of L-Pten KO in the immunoblotting, while we found detectable UCP-1 in BAT, such content that decreased upon aging and progression of liver disease. Next, we evaluated UCP-1-dependent thermogenic capacity in 8- and 48-week-old L-Pten WT and KO by evaluating mouse oxygen consumption at

thermoneutral conditions (30 °C) in response to a challenge with the β3 adrenergic receptor agonist CL-316,243. As depicted in Fig. 4B, 8-week-old L-Pten WT and L-Pten KO displayed similar oxygen consumption rates in response to the CL-316,243 injection, indicating similar thermogenic capacity between groups. In contrast, 48-week-old L-Pten KO featured a severely impaired thermogenic capacity, as evidenced by the smaller increase in whole-body oxygen consumption and core body temperature in response to CL-316,243 than those displayed by littermates L-Pten WT (Fig. 4C, D, respectively). Altogether, these findings indicate that UCP-1-mediated thermogenic capacity is markedly reduced in 48-week-old L-Pten KO mice.

Next, we investigated the impact of those changes in thermogenic capacity on whole-body and tissue energy expenditure through indirect calorimetry (oxygen consumption). As illustrated in Fig. 5A, 8-week-old L-Pten KO displayed increased oxygen consumption and respiratory exchange ratio (RER), but no changes in locomotor activity, indicating increased energy expenditure and utilization of carbohydrates as a substrate for energy production. There were no significant changes in oxygen consumption, locomotor activity, and RER in 24- and 48-week-old L-Pten KO (Fig. 5B, C). The relationship between oxygen consumption and body mass in 8- and 48-week-old mice was evaluated using ANCOVA and was found not significant (Supplementary Files 1 and 2). We also examined the individual contribution of tissues to whole-body energy expenditure. As illustrated in Fig. 5D, L-Pten KO displayed reduced liver rates of oxygen consumption expressed per mg of tissue at 8 and 48 weeks of age but increased whole-liver oxygen consumption at 24 and 48 weeks of age, which reflects organ contribution to whole-body energy expenditure. Similarly to the liver, L-Pten KO displayed reduced BAT rates of oxygen consumption expressed per mg of tissue at 24 and 48 weeks of age but increased whole-BAT oxygen consumption at 8, but not at 24 and 48 weeks of age (Fig. 5E). Regarding iWAT, on the other hand, L-Pten KO showed increased rates of oxygen consumption expressed per mg of tissue at 48 weeks but reduced whole-iWAT oxygen consumption at all ages investigated (Fig. 5F). Altogether, these findings indicate that HCC induced by Pten deletion in hepatocytes is associated with reduced BAT UCP-1 and thermogenic capacity, but no changes in energy expenditure.

Discussion

We tested herein the hypothesis that an enhanced BAT and iWAT UCP-1-mediated thermogenesis induced by high levels of FGF-21 are involved in the catabolic state and reduction in fat mass found upon HCC. Our main findings indicate that, despite high serum FGF-21 levels and iWAT browning, HCC induced by Pten deletion in hepatocytes is associated with reduced BAT UCP-1 content and expression of sympathetically-regulated genes GyK, LPL, and FATP, which altogether resulted in an impaired whole-body thermogenic capacity in response to CL-316,243. These findings strongly suggest that FGF-21 pro-thermogenic actions in BAT are context-dependent, not occurring upon NASH or HCC induced by hepatocyte Pten deletion, perhaps due to the reduced serum leptin, insulin, and adiponectin levels found in these conditions. Additionally, it can be concluded that UCP-1-mediated nonshivering thermogenesis is not a major energy-expending component of the catabolic process associated with HCC induced by Pten deletion in hepatocytes, such findings that are in accordance with studies in humans showing that brown fat thermogenesis is not involved with cancer-associated cachexia and does not affect survival in patients suffering with cachexia [15, 4].

Confirming and extending previous findings [21, 52], Pten deletion in hepatocytes was associated with a marked and progressive increase in liver mass and lipid accumulation culminating with NASH and HCC appearance in 24- and 48-week-old mice, respectively. Interestingly, the marked increase in liver mass in HCC was not associated with major changes in mouse body weight, likely due to the compensatory reductions in adipose tissue and skeletal muscle masses, which are common manifestations of a cancer-related catabolic state. Of note, HCC-related reduction in muscle and adipose tissue masses, which cannot be attributed to changes in food intake, may be related to catabolic signals secreted by the liver along the reduced serum levels of insulin, a growth factor that displays anabolic actions on muscle mass.

One liver-derived putative candidate to mediate HCC actions is FGF-21, a hepatokine whose liver and serum contents were markedly increased during the NAFLD progression induced by Pten deletion in the hepatocyte, reaching its highest levels upon HCC. Indeed, FGF-21 has been shown to act as a robust marker of NAFLD in both rodents and humans [14, 58, 57], to promote adipose tissue lipolysis in vivo under specific conditions [22, 49], and to mediate both the muscle atrophy induced by fasting [41] and the improvement in insulin sensitivity displayed by L-Pten KO mice [5]. Similarly to lipolysis, FGF-21 was also shown in specific conditions to promote BAT and iWAT UCP-1-mediated thermogenesis increasing energy expenditure and thus counteracting obesity and NAFLD development in mice [45, 59, 12, 56]. Indeed, we found that upon HCC, elevated serum FGF-21 was associated with increased UCP-1 and GyK mRNA levels and the appearance of multilocular adipocytes in iWAT, indicating enhanced tissue browning. But surprisingly, and in contrast to iWAT, high FGF-21 levels were also associated with increased lipid

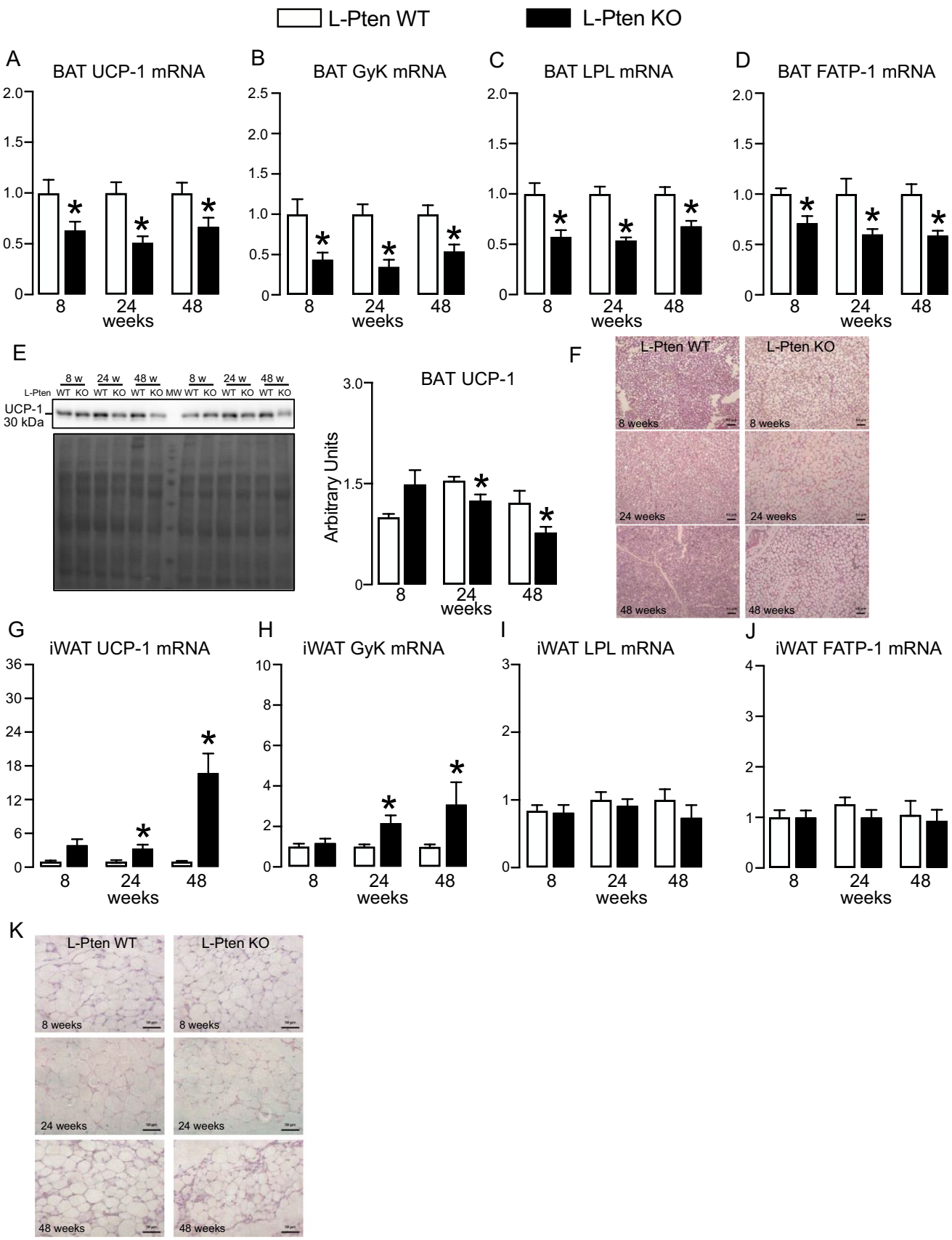
L-Pten WT
L-Pten KO
A
BAT UCP-1 mRNA
B
BAT GyK mRNA
C
BAT LPL mRNA
D
BAT FATP-1 mRNA
8
24
48
weeks
E
8 w
24 w
48 w
L-Pten WT KO WT KO WT KO MW WT KO WT KO WT KO
UCP-1
30 kDa
BAT UCP-1
Arbitrary Units
F
L-Pten WT
L-Pten KO
8 weeks
24 weeks
48 weeks
G
iWAT UCP-1 mRNA
H
iWAT GyK mRNA
I
iWAT LPL mRNA
J
iWAT FATP-1 mRNA
K
L-Pten WT
L-Pten KO
8 weeks
24 weeks
48 weeks

◂**Fig. 3** Liver cancer reduces BAT UCP-1 content but promotes iWAT browning. Brown adipose tissue (BAT) uncoupling protein 1 (UCP-1) (**A**), glycerol kinase (GyK) (**B**), lipoprotein lipase (LPL) (**C**), fatty acid transporter 1 (FATP-1) (**D**) mRNA levels, UCP-1 protein content (**E**), histology by H/E staining (**F**), and inguinal white adipose tissue (iWAT) UCP-1 (**G**), GyK (**H**), LPL (**I**), and FATP-1 (**J**) mRNA levels and histology by H/E staining (**K**) in 8, 24 and 48-week-old Pten floxed (L-Pten WT) and Pten floxed albumin cre$^{+/-}$ (L-Pten KO) mice bearing Pten deletion in hepatocytes. Results are expressed as mean ± SEM. n = 6-10 mice per group. Student's t-test was used to analyze the effects of Pten deletion (same age L-Pten WT vs L-Pten KO). *$p \leq 0.05$

deposition and reduced UCP-1 content and expression of the sympathetic-regulated proteins GyK, LPL, and FATP-1 in BAT [16, 28, 6], all suggestive of reduced BAT sympathetic activity and thermogenesis. One interesting question that arises from these findings is whether iWAT browning could compensate for the reduced BAT UCP-1 content seen upon HCC. The markedly lower, non-detected UCP-1 content in iWAT in comparison to readily detectable in BAT in the immunoblotting along with the impaired thermogenic capacity of 48-week-old L-Pten KO mice evaluated in response to CL-316,243 strongly indicate that an enhanced iWAT browning cannot compensate for the reduced BAT UCP-1 content and thermogenesis in this condition. These findings are in agreement with several studies showing a minimal contribution of iWAT browning to mice thermogenic capacity and energy expenditure in vivo [7, 8, 30, 31, 48] and exclude a possible implication of UCP-1-mediated thermogenesis in HCC-associated catabolic state and cachexia. Corroborating our findings, two recent studies found through fluoro-deoxyglucose (^{18}F-FDG) positron emission tomography (PET) scans of large human cohorts that BAT is not associated with cancer-associated cachexia and does not worsen overall survival in patients with cachexia [15, 4].

Noteworthy, these changes in iWAT and BAT UCP-1 content and thermogenic capacity seen upon HCC also did not impact energy expenditure in mice, as evidenced by the similar rates of oxygen consumption displayed by 48-week-old

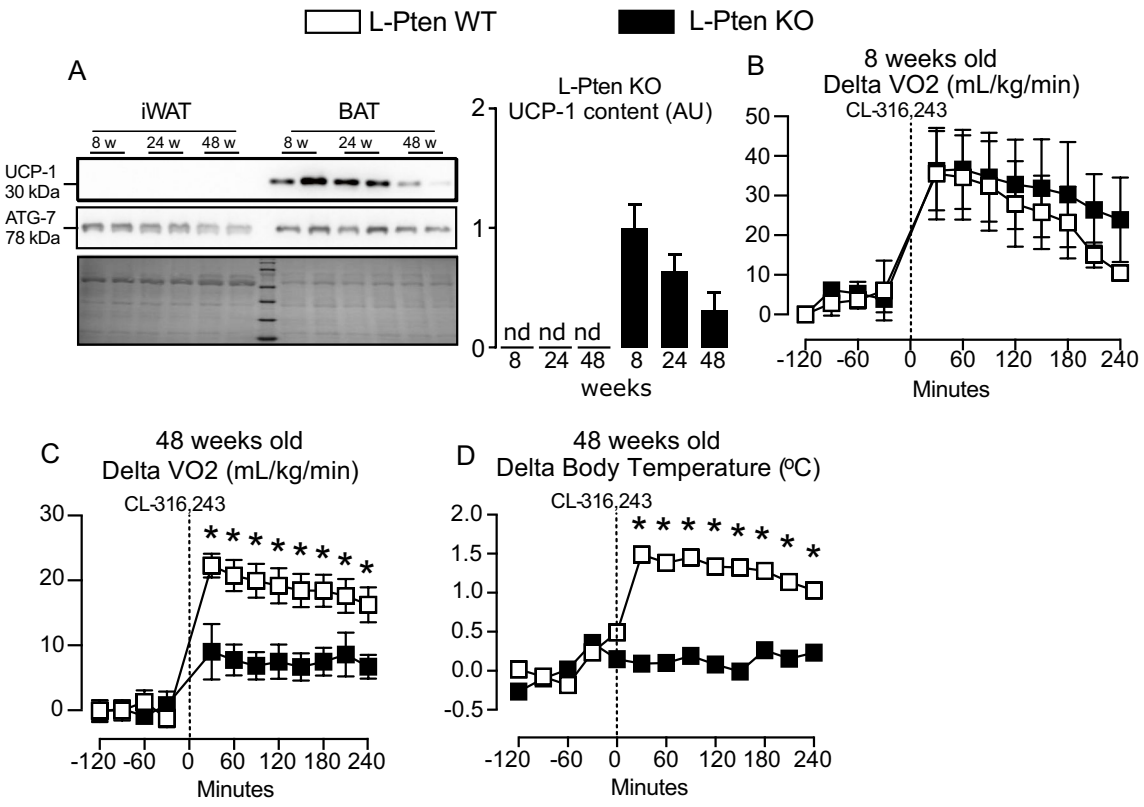

Fig. 4 Liver cancer reduces UCP-1-mediated thermogenic capacity. Inguinal white adipose tissue (iWAT) and brown adipose tissue (BAT) uncoupling protein 1 (UCP-1) content in 8-, 24-, and 48-week-old Pten floxed albumin cre$^{+/-}$ (L-Pten KO) mice (**A**), delta of whole-body oxygen consumption in 8- and 48-week-old Pten floxed (L-Pten WT) and L-Pten KO (**B**, **C**), and delta of core temperature (**D**) in 48-week-old L-Pten WT and L-Pten KO mice evaluated at thermoneutral conditions (30 °C) in response to CL316,243 (1 mg/ kg of body weight). Results are expressed as mean ± SEM. n = 4-8 mice per group. Student's t-test was used to analyze the effects of Pten deletion (same age L-Pten WT vs L-Pten KO). *$p \leq 0.05$

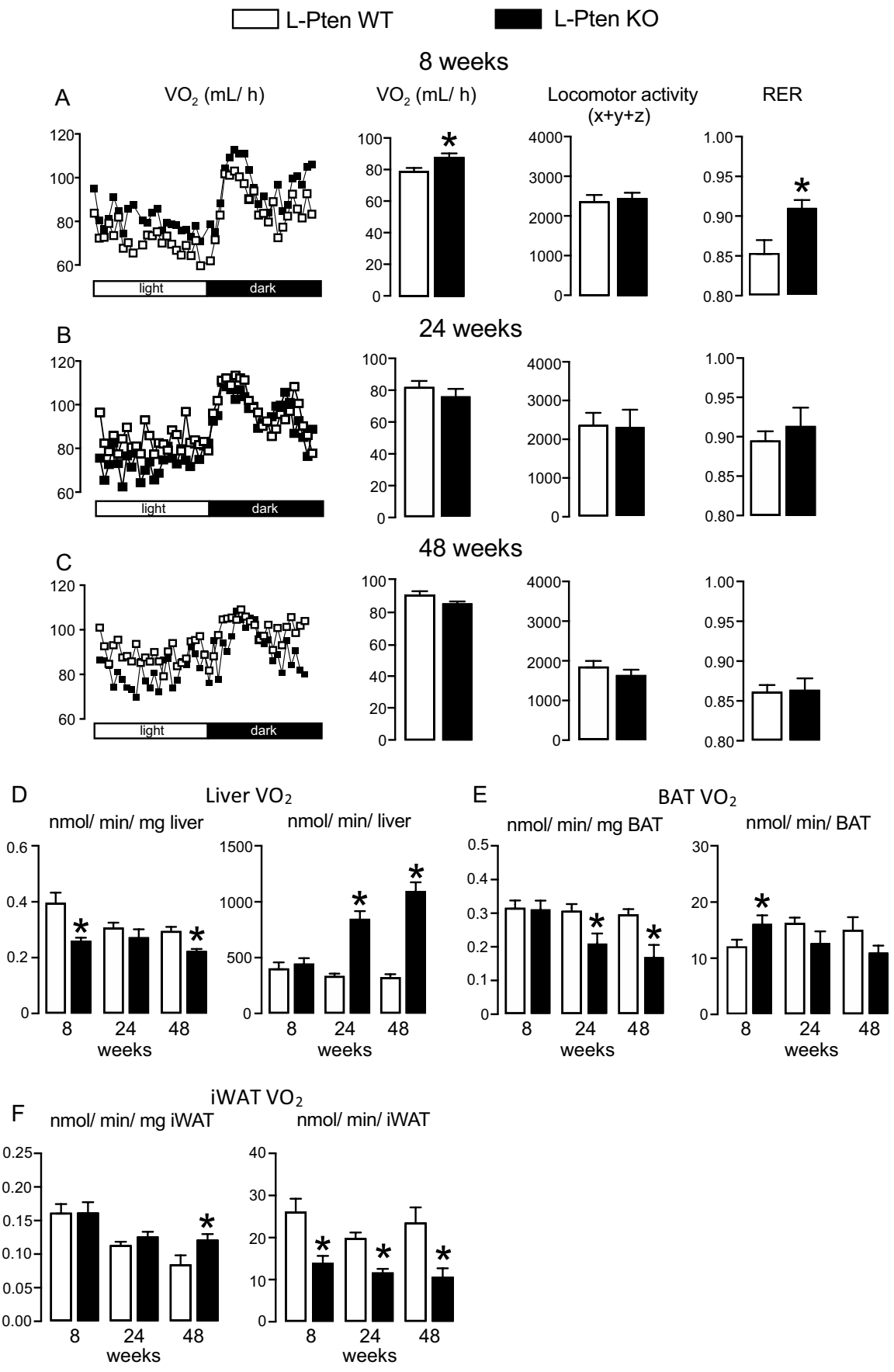
L-Pten WT
L-Pten KO
8 weeks
A
VO2 (mL/ h)
VO2 (mL/ h)
Locomotor activity (x+y+z)
RER
light
dark
24 weeks
B
48 weeks
C
D
Liver VO2
nmol/ min/ mg liver
nmol/ min/ liver
E
BAT VO2
nmol/ min/ mg BAT
nmol/ min/ BAT
F
iWAT VO2
nmol/ min/ mg iWAT
nmol/ min/ iWAT
weeks

◂**Fig. 5** Liver cancer does not affect whole-body energy expenditure. Whole-body oxygen consumption (VO2), locomotor activity, respiratory exchange ratio (RER) (**A**–**C**), liver (**D**), brown adipose tissue (BAT) (**E**), and inguinal white adipose tissue (iWAT) (**F**) oxygen consumption expressed by mg of tissue and total tissue in 8-, 24-, and 48-week-old Pten floxed (L-Pten WT) and Pten floxed albumin cre$^{+/-}$ (L-Pten KO) mice bearing Pten deletion in hepatocytes. Results are expressed as mean ± SEM. $n = 6$–10 mice per group. Student's *t*-test was used to analyze the effects of Pten deletion (same age L-Pten WT vs L-Pten KO). *$p \leq 0.05$

L-Pten KO and WT; such findings are surprising, considering the important contribution of BAT thermogenesis to energy expenditure in mice acclimated to 23 °C, a temperature below the thermoneutral zone. One possible reason to explain this may be the marked increase in liver oxygen consumption found upon HCC that may compensate for the reduced BAT thermogenesis and oxygen consumption. In humans, cirrhosis and HCC have been associated with mixed results regarding energy expenditure with reports of reductions, no changes, or increases, such discrepancies that seem to be related to the cause and stage of the disease, patient sex, and lean mass, among other factors [36, 39]. Importantly, the contribution of UCP-1-mediated nonshivering thermogenesis to energy expenditure in HCC patients may be lower than that seen in rodents considering their smaller relative amounts of brown fat and that humans spend most of their lives under thermoneutral conditions.

Another interesting question that emerges from our findings is why high FGF-21 levels promote UCP-1-mediated thermogenesis and energy expenditure in some conditions such as diet-induced obesity [12, 56], but not others such as fasting [2, 24] and NAFLD induced by Pten deletion in hepatocytes shown here. One possibility is that these FGF-21 actions are context-dependent requiring other signaling molecules enriched upon diet-induced obesity, but not fasting or NAFLD induced by Pten deletion in hepatocytes. In this sense, a recent study has shown that FGF-21 signals through leptin receptor-expressing cells to regulate body weight, and that central leptin signaling is required for FGF-21 full effects to increase energy expenditure and reduce body weight [10]. Indeed, we found in our study that serum leptin levels are significantly reduced in L-Pten KO mice in all ages investigated. In addition to leptin, serum levels of insulin and adiponectin, hormones previously shown to regulate energy balance and sympathetic activity to BAT and iWAT [43, 35], were also markedly reduced in L-Pten KO mice upon NASH and HCC. While this reduction in serum insulin is expected considering the increase in insulin sensitivity induced by FGF-21 in L-Pten KO mice [5], that of adiponectin is not in view of the previous findings that FGF-21 strongly induces the secretion of this adipokine [33, 20]. Indeed, FGF-21 not only stimulates adiponectin secretion, but also requires this adipokine to exert its actions on energy expenditure and glucose homeostasis [33, 20]. Whether leptin, insulin, and/or adiponectin are the missing mediators required for the translation of high serum FGF-21 levels into higher rates of UCP-1-mediated thermogenesis and energy expenditure in NAFLD induced by Pten deletion in hepatocytes will be addressed in future studies.

This study has important limitations. Despite being a recurrent signature in NASH and HCC [18, 47, 53], Pten loss of function in hepatocytes promotes a NAFL-NASH-HCC progression in mice that does not reproduce some frequent phenotypes seen in the NAFLD-associated with obesity, namely, insulin resistance, hyperglycemia, and hyperinsulinemia. Therefore, generalizations of our findings to other types and models of NAFLD including those associated with obesity should be done carefully.

In conclusion, our main findings indicate that FGF-21 pro-thermogenic actions in BAT are context-dependent not occurring upon HCC induced by Pten deletion in hepatocytes. Furthermore, our findings indicate that UCP-1-mediated nonshivering thermogenesis is not an important energy-expending component of the catabolic state associated with HCC induced by Pten deletion in hepatocytes. Future studies will address whether these phenotypes apply to different models of NAFLD including those associated with obesity in which reduced serum adiponectin and central leptin and insulin resistance may also affect FGF-21 pro-thermogenic actions.

Supplementary Information The online version contains supplementary material available at https://doi.org/10.1007/s13105-023-00970-4.

Acknowledgements The oxygen consumption ANCOVA analysis was provided by the NIDDK Mouse Metabolic Phenotyping Centers (MMPC, www.mmpc.org) using their Energy Expenditure Analysis page (http://www.mmpc.org/shared/regression.aspx) and supported by grants DK076169 and DK115255.

Author contribution A.S.P., M.F.M., E.C., L.A.P., T.B., T.E.O., T.S.V., B.F.L., M.O-S., G.R.G., C.A.T., and L.P.S.J. performed the experiments and collected and analyzed the data. A.A.S. and E.H.M. performed the analysis of thermogenic capacity. W.F. performed the experiments, collected and analyzed the data, and wrote the paper. All authors revised the manuscript and declare that all data were generated in-house and that no paper mill was used.

Funding This work was supported by grants from the São Paulo Research Foundation (FAPESP #15/19530-5, 19/01763-4, and 20/04159-8) and the Brazilian National Council for Scientific and Technological Development (CNPq #301756/2019-8 and #303784/2022-9) to W.F. and FAPESP to A.A.S. (#2018/03418-0). A.S.P. (#2017/23040-9 and 2022/02123-1), M.F.M. (#2017/17582-3), E.C. (#2020/166566), L.A.P. (#2019/17660-0), T.B. (#2015/22983-1), T.E.O. (#2019/04271-5), T.S.V. (#2020/10215-8), B.F.L. (#2021/14419-0), M. O-S. (#2017/12260-8), and E.H.M (#2020/09399-7) were recipients of a Ph.D. studentship from FAPESP. G.R.G. and C.A.T. were recipients of Ph.D. fellowship from CNPq and

Coordenação de Aperfeiçoamento de Pessoal de Nível Superior (CAPES), respectively.

Data availability Authors agree to make any materials, data, code, and associated protocols available upon request.

Declarations

Conflict of Interest The authors declare no competing interests.

References

1. Albhaisi S, Chowdhury A, Sanyal AJ (2019) Non-alcoholic fatty liver disease in lean individuals. JHEP Rep 1:329. https://doi.org/10.1016/J.JHEPR.2019.08.002
2. Badman MK, Pissios P, Kennedy AR et al (2007) Hepatic fibroblast growth factor 21 is regulated by PPARalpha and is a key mediator of hepatic lipid metabolism in ketotic states. Cell Metab 5:426–437. https://doi.org/10.1016/J.CMET.2007.05.002
3. Bae JJ, Rho JW, Lee TJ et al (2007) Loss of heterozygosity on chromosome 10q23 and mutation of the phosphatase and tensin homolog deleted from chromosome 10 tumor suppressor gene in Korean hepatocellular carcinoma patients. Oncol Rep 18:1007–1013. https://doi.org/10.3892/or.18.4.1007
4. Becker AS, Zellweger C, Bacanovic S et al (2020) Brown fat does not cause cachexia in cancer patients: a large retrospective longitudinal FDG-PET/CT cohort study. PLoS One 15(10):e0239990. https://doi.org/10.1371/journal.pone.0239990
5. Berthou F, Sobolewski C, Abegg D et al (2022) Hepatic PTEN signaling regulates systemic metabolic homeostasis through hepatokines-mediated liver-to-peripheral organs crosstalk. Int J Mol Sci 23(7):3959. https://doi.org/10.3390/IJMS23073959
6. Cannon B, Nedergaard J (2004) Brown adipose tissue: function and physiological significance. Physiol Rev 84:277–359. https://doi.org/10.1152/PHYSREV.00015.2003
7. Castro E, Silva TEO, Festuccia WT (2017) Critical review of beige adipocyte thermogenic activation and contribution to whole-body energy expenditure. Horm Mol Biol Clin Investig 31(2):20170042. https://doi.org/10.1515/hmbci-2017-0042
8. Castro É, Vieira TS, Oliveira TE et al (2021) Adipocyte-specific mTORC2 deficiency impairs BAT and iWAT thermogenic capacity without affecting glucose uptake and energy expenditure in cold-acclimated mice. Am J Physiol Endocrinol Metab 321:E592–E605. https://doi.org/10.1152/AJPENDO.00587.2020
9. Chimin P, Andrade ML, Belchior T et al (2017) Adipocyte mTORC1 defciency promotes adipose tissue inflammation and NLRP3 inflammasome activation via oxidative stress and de novo ceramide synthesis. J Lipid Res 58(9):1797–1807. https://doi.org/10.1194/jlr.M074518
10. Claflin KE, Sullivan AI, Naber MC et al (2022) Pharmacological FGF21 signals to glutamatergic neurons to enhance leptin action and lower body weight during obesity. Mol Metab 64:101564. https://doi.org/10.1016/J.MOLMET.2022.101564
11. Clifford RJ, Zhang J, Meerzaman DM et al (2010) Genetic variations at loci involved in the immune response are risk factors for hepatocellular carcinoma. Hepatology 52:2034–2043. https://doi.org/10.1002/HEP.23943
12. Coskun T, Bina HA, Schneider MA et al (2008) Fibroblast growth factor 21 corrects obesity in mice. Endocrinology 149:6018–6027. https://doi.org/10.1210/EN.2008-0816
13. de Jong JMA, Larsson O, Cannon B, Nedergaard J (2015) A stringent validation of mouse adipose tissue identity markers. Am J Physiol Endocrinol Metab 308:E1085–E1105. https://doi.org/10.1152/AJPENDO.00023.2015
14. Dushay J, Chui PC, Gopalakrishnan GS et al (2010) Increased fibroblast growth factor 21 in obesity and nonalcoholic fatty liver disease. Gastroenterology 139:456–463. https://doi.org/10.1053/J.GASTRO.2010.04.054
15. Eljalby M, Huang X, Becher T et al (2023) Brown adipose tissue is not associated with cachexia or increased mortality in a retrospective study of patients with cancer. Am J Physiol Endocrinol Metab 324:E144–E153. https://doi.org/10.1152/AJPENDO.00187.2022
16. Festuccia WTL, Guerra-Sá R, Kawashita NH et al (2003) Expression of glycerokinase in brown adipose tissue is stimulated by the sympathetic nervous system. Am J Physiol Regul Integr Comp Physiol 284(6):R1536–R1541. https://doi.org/10.1152/ajpregu.00764.2002
17. Fisher Ffolliott M, Kim MS, Doridot L et al (2016) A critical role for ChREBP-mediated FGF21 secretion in hepatic fructose metabolism. Mol Metab 6:14–21. https://doi.org/10.1016/J.MOLMET.2016.11.008
18. Govaere O, Cockell S, Tiniakos D et al (2020) Transcriptomic profiling across the nonalcoholic fatty liver disease spectrum reveals gene signatures for steatohepatitis and fibrosis. Sci Transl Med 12(572):eaba4448. https://doi.org/10.1126/SCITRANSLMED.ABA4448
19. Han J, Meng Q, Shen L, Wu G (2018) Interleukin-6 induces fat loss in cancer cachexia by promoting white adipose tissue lipolysis and browning. Lipids Health Dis 17:1–8. https://doi.org/10.1186/S12944-018-0657-0/FIGURES/3
20. Holland WL, Adams AC, Brozinick JT et al (2013) An FGF21-adiponectin-ceramide axis controls energy expenditure and insulin action in mice. Cell Metab 17:790–797. https://doi.org/10.1016/J.CMET.2013.03.019
21. Horie Y, Suzuki A, Kataoka E et al (2004) Hepatocyte-specific Pten deficiency results in steatohepatitis and hepatocellular carcinomas. J Clin Invest 113:1774–1783. https://doi.org/10.1172/JCI20513
22. Hotta Y, Nakamura H, Konishi M et al (2009) Fibroblast growth factor 21 regulates lipolysis in white adipose tissue but is not required for ketogenesis and triglyceride clearance in liver. Endocrinology 150:4625–4633. https://doi.org/10.1210/EN.2009-0119
23. Hu TH, Huang CC, Lin PR et al (2003) Expression and prognostic role of tumor suppressor gene PTEN/MMAC1/TEP1 in hepatocellular carcinoma. Cancer 97:1929–1940. https://doi.org/10.1002/CNCR.11266
24. Inagaki T, Dutchak P, Zhao G et al (2007) Endocrine regulation of the fasting response by PPARalpha-mediated induction of fibroblast growth factor 21. Cell Metab 5:415–425. https://doi.org/10.1016/J.CMET.2007.05.003
25. Jensen-Cody SO, Potthoff MJ (2021) Hepatokines and metabolism: deciphering communication from the liver. Mol Metab 44:101138. https://doi.org/10.1016/J.MOLMET.2020.101138
26. Kaiyala KJ (2014) Mathematical model for the contribution of individual organs to non-zero y-intercepts in single and multi-compartment linear models of whole-body energy expenditure. PLoS One 9:e103301. https://doi.org/10.1371/JOURNAL.PONE.0103301
27. Kaiyala KJ, Morton GJ, Leroux BG et al (2010) Identification of body fat mass as a major determinant of metabolic rate in mice. Diabetes 59:1657–1666. https://doi.org/10.2337/DB09-1582
28. Kawashita NH, Festuccia WTL, Brito MN et al (2002) Glycerokinase activity in brown adipose tissue: a sympathetic regulation? Am J Physiol Regul Integr Comp Physiol 282(4):R1185–R1190. https://doi.org/10.1152/ajpregu.00419.2001
29. Kir S, White JP, Kleiner S et al (2014) Tumour-derived PTH-related protein triggers adipose tissue browning and cancer

cachexia. Nature 513(7516):100–104. https://doi.org/10.1038/nature13528
30. Labbé SM, Caron A, Chechi K et al (2016) Metabolic activity of brown, "beige," and white adipose tissues in response to chronic adrenergic stimulation in male mice. Am J Physiol Endocrinol Metab 311:E260–E268. https://doi.org/10.1152/AJPENDO.00545.2015
31. Labbé SM, Caron XA, Festuccia WT et al (2018) Interscapular brown adipose tissue denervation does not promote the oxidative activity of inguinal white adipose tissue in male mice. Am J Physiol Endocrinol Metab 315:E815–E824. https://doi.org/10.1152/AJPENDO.00210.2018
32. Liang W, Menke AL, Driessen A et al (2014) Establishment of a general NAFLD scoring system for rodent models and comparison to human liver pathology. PLoS One 9(12):e115922. https://doi.org/10.1371/JOURNAL.PONE.0115922
33. Lin Z, Tian H, Lam KSL et al (2013) Adiponectin mediates the metabolic effects of FGF21 on glucose homeostasis and insulin sensitivity in mice. Cell Metab 17:779–789. https://doi.org/10.1016/J.CMET.2013.04.005
34. Magdalon J, Chimin P, Belchior T et al (2016) Constitutive adipocyte mTORC1 activation enhances mitochondrial activity and reduces visceral adiposity in mice. Biochim Biophys Acta Mol Cell Biol Lipids 1861. https://doi.org/10.1016/j.bbalip.2016.02.023
35. Masaki T, Chiba S, Yasuda T et al (2003) Peripheral, but not central, administration of adiponectin reduces visceral adiposity and upregulates the expression of uncoupling protein in agouti yellow (Ay/a) obese mice. Diabetes 52:2266–2273. https://doi.org/10.2337/DIABETES.52.9.2266
36. McCullough AJ, Raguso C (1999) Effect of cirrhosis on energy expenditure. Am J Clin Nutr 69:1066–1068. https://doi.org/10.1093/AJCN/69.6.1066
37. Mouchiroud M, Camiré É, Aldow M et al (2019) The hepatokine TSK does not affect brown fat thermogenic capacity, body weight gain, and glucose homeostasis. Mol Metab 30:184–191. https://doi.org/10.1016/j.molmet.2019.09.014
38. Mouchiroud M, Camiré É, Aldow M et al (2019) The hepatokine Tsukushi is released in response to NAFLD and impacts cholesterol homeostasis. JCI Insight 4(15). https://doi.org/10.1172/jci.insight.129492
39. Müller MJ, Böttcher J, Selberg O et al (1999) Hypermetabolism in clinically stable patients with liver cirrhosis. Am J Clin Nutr 69:1194–1201. https://doi.org/10.1093/AJCN/69.6.1194
40. Oliveira TE, Castro É, Belchior T et al (2019) Fish oil protects wild type and uncoupling protein 1-deficient mice from obesity and glucose intolerance by increasing energy expenditure. Mol Nutr Food Res 63. https://doi.org/10.1002/mnfr.201800813
41. Oost LJ, Kustermann M, Armani A et al (2019) Fibroblast growth factor 21 controls mitophagy and muscle mass. J Cachexia Sarcopenia Muscle 10:630–642. https://doi.org/10.1002/JCSM.12409
42. Ortega-Molina A, Efeyan A, Lopez-Guadamillas E et al (2012) Pten positively regulates brown adipose function, energy expenditure, and longevity. Cell Metab 15:382–394. https://doi.org/10.1016/J.CMET.2012.02.001
43. Rahmouni K, Morgan DA, Morgan GM et al (2004) Hypothalamic PI3K and MAPK differentially mediate regional sympathetic activation to insulin. J Clin Invest 114:652–658. https://doi.org/10.1172/JCI21737
44. Rinella ME (2015) Nonalcoholic fatty liver disease: a systematic review. JAMA 313:2263–2273. https://doi.org/10.1001/JAMA.2015.5370
45. Sáenz de Urturi D, Buqué X, Porteiro B et al (2022) Methionine adenosyltransferase 1a antisense oligonucleotides activate the liver-brown adipose tissue axis preventing obesity and associated hepatosteatosis. Nat Commun 13:1096. https://doi.org/10.1038/S41467-022-28749-Z
46. Sanders FWB, Griffin JL (2016) De novo lipogenesis in the liver in health and disease: more than just a shunting yard for glucose. Biol Rev Camb Philos Soc 91:452–468. https://doi.org/10.1111/BRV.12178
47. Schulze K, Imbeaud S, Letouzé E et al (2015) Exome sequencing of hepatocellular carcinomas identifies new mutational signatures and potential therapeutic targets. Nat Genet 47:505–511. https://doi.org/10.1038/NG.3252
48. Shabalina IG, Petrovic N, deJong JMA et al (2013) UCP1 in brite/beige adipose tissue mitochondria is functionally thermogenic. Cell Rep 5:1196–1203. https://doi.org/10.1016/J.CELREP.2013.10.044
49. She QY, Bao JF, Wang HZ et al (2022) Fibroblast growth factor 21: A "rheostat" for metabolic regulation? Metabolism 130:155166. https://doi.org/10.1016/J.METABOL.2022.155166
50. Shellock FG, Riedinger MS, Fishbein MC (1986) Brown adipose tissue in cancer patients: possible cause of cancer-induced cachexia. J Cancer Res Clin Oncol 111:82–85. https://doi.org/10.1007/BF00402783
51. Steiner AA, Flatow EA, Brito CF et al (2017) Respiratory gas exchange as a new aid to monitor acidosis in endotoxemic rats: relationship to metabolic fuel substrates and thermometabolic responses. Physiol Rep 5:e13100. https://doi.org/10.14814/PHY2.13100
52. Stiles B, Wang Y, Stahl A et al (2004) Liver-specific deletion of negative regulator Pten results in fatty liver and insulin hypersensitivity [corrected]. Proc Natl Acad Sci USA 101:2082–2087. https://doi.org/10.1073/PNAS.0308617100
53. Vinciguerra M, Veyrat-Durebex C, Moukil MA et al (2008) PTEN down-regulation by unsaturated fatty acids triggers hepatic steatosis via an NF-kappaBp65/mTOR-dependent mechanism. Gastroenterology 134:268–280. https://doi.org/10.1053/J.GASTRO.2007.10.010
54. Vitali A, Murano I, Zingaretti MC et al (2012) The adipose organ of obesity-prone C57BL/6J mice is composed of mixed white and brown adipocytes. J Lipid Res 53:619–629. https://doi.org/10.1194/JLR.M018846
55. Wang Q, Sharma VP, Shen H et al (2019) The hepatokine Tsukushi gates energy expenditure via brown fat sympathetic innervation. Nature Metabolism 1(2):251–260. https://doi.org/10.1038/s42255-018-0020-9
56. Xu J, Lloyd DJ, Hale C et al (2009) Fibroblast growth factor 21 reverses hepatic steatosis, increases energy expenditure, and improves insulin sensitivity in diet-induced obese mice. Diabetes 58:250–259. https://doi.org/10.2337/DB08-0392
57. Yang C, Lu W, Lin T et al (2013) Activation of liver FGF21 in hepatocarcinogenesis and during hepatic stress. BMC Gastroenterol 13:1–14. https://doi.org/10.1186/1471-230X-13-67/FIGURES/8
58. Yilmaz Y, Eren F, Yonal O et al (2010) Increased serum FGF21 levels in patients with nonalcoholic fatty liver disease. Eur J Clin Invest 40:887–892. https://doi.org/10.1111/J.1365-2362.2010.02338.X
59. Zouhar P, Janovska P, Stanic S et al (2021) A pyrexic effect of FGF21 independent of energy expenditure and UCP1. Mol Metab 53. https://doi.org/10.1016/J.MOLMET.2021.101324